

The critical radiation intensity for direct collapse black hole formation: dependence on the radiation spectral shape

Kazuyuki Sugimura,^{1*} Kazuyuki Omukai¹ and Akio K. Inoue²

¹*Astronomical Institute, Tohoku University, Aoba, Sendai 980-8578, Japan*

²*College of General Education, Osaka Sangyo University, Daito, Osaka 574-8530, Japan*

16 July 2014

ABSTRACT

It has been proposed that supermassive black holes (SMBHs) are originated from direct-collapse black holes (DCBHs) that are formed at $z \gtrsim 10$ in the primordial gas in the case that H_2 cooling is suppressed by strong external radiation. In this work, we study the critical specific intensity J^{crit} required for DCBH formation for various radiation spectral shapes by a series of one-zone calculations of a collapsing primordial-gas cloud. We calculate the critical specific intensity at the Lyman-Werner (LW) bands $J_{\text{LW},21}^{\text{crit}}$ (in units of $10^{-21} \text{ erg s}^{-1} \text{ Hz}^{-1} \text{ sr}^{-1} \text{ cm}^{-2}$) for realistic spectra of metal-poor galaxies. We find J^{crit} is not sensitive to the age or metallicity for the constant star formation galaxies with $J_{\text{LW},21}^{\text{crit}} = 1300 - 1400$, while J^{crit} decreases as galaxies become older or more metal-enriched for the instantaneous starburst galaxies. However, such dependence for the instantaneous starburst galaxies is weak for the young or extremely metal-poor galaxies: $J_{\text{LW},21}^{\text{crit}} = 1000 - 1400$ for the young (the age less than 100 Myr) galaxies and $J_{\text{LW},21}^{\text{crit}} \approx 1400$ for the extremely metal-poor ($Z < 5 \times 10^{-4} Z_{\odot}$) galaxies. We also find J^{crit} is solely determined by the ratio of the H^- and H_2 photodissociation rate coefficients $k_{\text{H}^-, \text{pd}}/k_{\text{H}_2, \text{pd}}$, with which we develop a formula to estimate J^{crit} for a given spectrum. The typical value of J^{crit} for the realistic spectra is higher than those expected in the literature, which affects the estimated DCBH number density n_{DCBH} . By extrapolating the result of Dijkstra, Ferrara & Mesinger, we obtain $n_{\text{DCBH}} \sim 10^{-10} \text{ cMpc}^{-3}$ at $z = 10$, although there is still large uncertainty in this estimation. This estimated n_{DCBH} is roughly consistent with the observed number density of high-redshift SMBHs $n_{\text{SMBH}} \sim 10^{-9} \text{ cMpc}^{-3}$ at $z \sim 6$, considering uncertainties, but much less than that of present-day SMBHs $n_{\text{SMBH}} \sim 10^{-4} \text{ cMpc}^{-3}$, indicating other seed BH formation mechanisms are also operating.

Key words: quasars: supermassive black holes - cosmology: theory - galaxies: high-redshift.

1 INTRODUCTION

Observations reveal that almost all galaxies host supermassive black holes (SMBHs) at their centers (Ferrarese & Merritt (2000); Gebhardt et al. (2000); Gültekin et al. (2009)). Although SMBHs play an important role in the cosmic history by their radiative activities via accretion of surrounding gas, their origin is remained one of the most puzzling mysteries in astrophysics. The discovery of SMBHs with inferred black hole mass $> 10^9 M_{\odot}$ at $z > 6$ (Fan et al. (2001); Mortlock (2012); Venemans et al. (2013)) suggests that SMBH seeds are formed very early in the history of the Universe. In order for remnants of first generation (pop III)

stars ($M_{\text{popIII}} \sim 100 M_{\odot}$) to be seeds of SMBHs, surrounding gas is needed to accrete at the Eddington limited rate for the entire period of accretion from $\sim 100 M_{\odot}$ to $> 10^9 M_{\odot}$. However, the Eddington limited accretion is likely to be prevented by radiative feedback (Johnson & Bromm (2007); Alvarez et al. (2009); Milosavljević et al. (2009)).

A possible solution to this problem is that SMBH seeds are not remnants of pop III stars but direct collapse black holes (DCBHs) that are formed by direct collapse of supermassive stars (SMSs) with mass $\gtrsim 10^5 M_{\odot}$ (Bromm & Loeb (2003)). SMSs are expected to be formed from primordial-gas clouds in halos with virial temperature $T_{\text{vir}} \gtrsim 10^4 \text{ K}$, in the case that the clouds collapse isothermally with the temperature of gas $T_{\text{gas}} \sim 8000 \text{ K}$ via atomic cooling in the absence of H_2 molecules due to strong external radiation

* E-mail: sugimura@astr.tohoku.ac.jp

(Omukai (2001) hereafter O01).¹ In such a case, it has been shown that fragmentation of the gas is suppressed (Bromm & Loeb (2003); Regan et al. (2007); Regan & Haehnelt (2009); Inayoshi et al. (2014)) and that the large accretion rate is expected to continue until SMSs (and subsequently DCBHs) are formed (Hosokawa et al. (2012, 2013)).

In this paper, we calculate the critical specific intensities of external radiation J^{crit} required for DCBH formation. External radiation reduces the abundance of H_2 in two ways: one is by direct photodissociation of H_2 with the Lyman-Werner (LW) photons (photons with energies $11.2 \text{ eV} < h\nu < 13.6 \text{ eV}$); the other is by photodissociation of the intermediary H^- of the dominant H_2 formation channel with the photons with energies $\gtrsim 0.76 \text{ eV}$. For the fixed spectral shape of radiation, J^{crit} is defined as the critical specific intensity $J_{\text{LW},21}^{\text{crit}} \equiv J_{21}^{\text{crit}}(h\nu = 12.4 \text{ eV})$ (in units of $10^{-21} \text{ erg s}^{-1} \text{ Hz}^{-1} \text{ sr}^{-1} \text{ cm}^{-2}$) at the center of the LW bands ($11.2 \text{ eV} < h\nu < 13.6 \text{ eV}$).² The critical intensity J^{crit} has been obtained in the various physical conditions, by using one-zone calculations (O01; Omukai et al. (2008); Inayoshi & Omukai (2011); Wolcott-Green & Haiman (2011)) or three-dimensional hydrodynamic simulations (Shang et al. (2010) hereafter S10; Latif et al. (2014)).

The feasibility of the SMBH formation scenario via DCBH can be tested by comparing the estimated DCBH number density n_{DCBH} with the observed high-redshift SMBH number density $n_{\text{SMBH}} \sim 10^{-9} \text{ cMpc}^{-3}$ at $z \sim 6$ (Fan et al. (2001); Venemans et al. (2013)). Although J^{crit} has wide range of varieties depending on physical conditions (O01; Omukai et al. (2008); S10; Inayoshi & Omukai (2011); Wolcott-Green & Haiman (2011); Latif et al. (2014)), they are in general much higher than the averaged cosmic LW background in the whole history of the Universe (see, e.g., O’Shea & Norman (2008); Johnson et al. (2013a)). To be concrete, $J_{\text{LW},21}^{\text{crit}} = O(10) - O(10^4)$ while $J_{\text{bg,LW},21} \lesssim 0.1$. Thus, $J > J^{\text{crit}}$ is achievable only in the rare situations that a primordial-gas cloud is irradiated by strong radiation from unusually nearby and/or bright galaxies, and the fraction of primordial-gas clouds with $T_{\text{vir}} \gtrsim 10^4 \text{ K}$ that can form DCBHs $f(J > J^{\text{crit}})$ is very small. In the literature (Dijkstra et al. (2008); Agarwal et al. (2012) hereafter A12; Agarwal et al. (2014); Dijkstra et al. (2014) hereafter D14; Yue et al. (2014)), $f(J > J^{\text{crit}})$ was obtained from semi-analytical calculations to estimate n_{DCBH} . They showed that the clouds with $J > J^{\text{crit}}$ are distributed at the high J tail of the probability density, and that even a small change in the value of J^{crit} causes significant difference to the predicted value of n_{DCBH} . Thus, precise determination of J^{crit} is very important in estimating n_{DCBH} .

It is known that J^{crit} strongly depends on the spectral shape of external radiation (O01). While $J_{\text{LW},21}^{\text{crit}} = O(10)$ for the black-body spectrum with $T_{\text{rad}} = 10^4 \text{ K}$ (S10), $J_{\text{LW},21}^{\text{crit}} = O(1000)$ for that with $T_{\text{rad}} = 10^5 \text{ K}$ (Wolcott-

Green et al. (2011) hereafter WG11). The black-body spectra with $T_{\text{rad}} = 10^4 \text{ K}$ and 10^5 K have frequently been used as approximate spectra of Pop II and Pop III galaxies, respectively, in the literature. However, the hardness of realistic spectra ranges between that of the above two black-body spectra (Leitherer et al. (1999); Schaerer (2003); Inoue (2011)), and thus actual values of J^{crit} realized in the Universe are not clear yet. In this paper, we study the dependence of J^{crit} on spectra and obtain J^{crit} for realistic spectra of galaxies calculated by the stellar population synthesis models (Schaerer (2003); Leitherer et al. (1999); Inoue (2011)).

This paper is organized as follows. In Sec. 2, we describe our one-zone model used to calculate the evolution of primordial-gas clouds under external radiation. In Sec. 3.1, we review physical processes proceeding during the evolution of the clouds, showing several results of our one-zone calculations. We determine J^{crit} for the black-body spectra with various temperatures in Sec. 3.2, and for realistic spectra in Sec. 3.3. In Sec. 3.4, we find the key parameter determining the dependence of J^{crit} on spectra, and develop a formula to estimate J^{crit} based on this parameter. Finally, we present the summary and discussion of this work in Sec. 4.

2 MODEL

2.1 Basics

In this paper, we use a one-zone model, as described in O01, to follow the gravitational collapse of primordial-gas clouds. By neglecting effects due to rotation or magnetic fields for simplicity, the gravitational collapse is expected to proceed like the self-similarity solution (Penston (1969); Larson (1969); Yahil (1983)). It has been confirmed that this simplified dynamical evolution actually describes the essential part of the gravitational collapse in three-dimensional hydrodynamic simulations (S10; Latif et al. (2014)). The quantities computed in one-zone models correspond to those in the nearly homogeneous central core of the self-similarity solution. The chemical, thermal and radiative processes are solved in detail. In the followings, we briefly explain the basics of our one-zone model, which is almost the same as the literature (O01; Omukai et al. (2008); S10), but with updated microphysics.

For the dynamical evolution, we assume the collapse of clouds proceeds as

$$\frac{d\rho_{\text{B}}}{dt} = \frac{\rho_{\text{B}}}{t_{\text{ff}}}, \quad (1)$$

where $t_{\text{ff}} \equiv \sqrt{3\pi/32G\rho}$ is the free-fall time, G the gravitational constant, $\rho = \rho_{\text{B}} + \rho_{\text{DM}}$ the total density, ρ_{B} the baryonic density and ρ_{DM} the dark matter (DM) density. We assume the evolution of ρ_{DM} is described by the spherical top-hat collapse model until ρ_{DM} reaches the virial density (see, e.g., O01). After that we keep ρ_{DM} constant. We assume the size of central core equals the Jeans length,

$$\lambda_{\text{J}} = \sqrt{\frac{\pi k T_{\text{gas}}}{G \rho_{\text{B}} \mu m_{\text{H}}}}, \quad (2)$$

where m_{H} is the proton mass, μ the mean molecular weight and k the Boltzmann constant.

¹ Other physical mechanism such as shock heating of gas (Inayoshi & Omukai (2012); Visbal et al. (2014a)) are proposed to suppress H_2 formation, but we concentrate on the case of strong external radiation in this paper.

² Some literature defined the critical specific intensity as $J_{\text{Lyc},21}^{\text{crit}} \equiv J_{21}^{\text{crit}}(h\nu = 13.6 \text{ eV})$ at the limit of the Lyman continuum (Lyc), but small difference in two definitions doesn’t matter in the order-of-magnitude argument in the introduction.

For the chemical evolution in primordial-gas clouds, we solve the chemical network of 9 species, H , H_2 , e , H^+ , H^- , H_2^+ , He , He^+ and He^{++} , with the chemical reaction rates of Glover & Abel (2008). In this work, we do not consider deuterium since the inclusion of it should make no difference to our results. Deuterium becomes important only in the situation that the gas is cooled below a few hundred Kelvin by HD cooling (see, e.g., Nagakura & Omukai (2005); McGreer & Bryan (2008); Nakauchi et al. (2014)). In the followings, we denote the number density of hydrogen nuclei as n , that of helium nuclei as n_{He} and that of species A as $n(A)$. We also denote the abundance of species A normalized by n as $y(A) \equiv n(A)/n$. The chemical evolution is affected by external radiation via photodissociation processes, which we explain in detail in Sec. 2.2.

The temperature evolution is described by the energy equation,

$$\frac{de}{dt} = -p \frac{d}{dt} \left(\frac{1}{\rho_B} \right) - \frac{\Lambda_{\text{net}}}{\rho_B}, \quad (3)$$

where $e = p/\rho_B(\gamma_{\text{ad}} - 1)$ is the internal energy per unit mass of baryon, $p = \rho_B k T_{\text{gas}}/\mu m_{\text{H}}$ the pressure and γ_{ad} the adiabatic exponent. The net cooling rate per unit volume Λ_{net} is given by $\Lambda_{\text{net}} = \Lambda_{\text{H}} + \Lambda_{\text{H}_2} + \Lambda_{\text{chem}}$, where Λ_{H} , Λ_{H_2} and Λ_{chem} are the cooling rates due to radiative cooling by $\text{Ly}\alpha$ (Anninos et al. (1997)) and H_2 (Glover & Abel (2008) with the LTE value by Hollenbach & McKee (1979)) and due to chemical reaction (Shapiro & Kang (1987)), respectively.

We start the calculation at the turnaround time, when the motion of the gas and DM turns from expansion to collapse. We assume that the turnaround time is at $z = 16$ and that initial values for physical quantities are given by $n = 4.5 \times 10^{-3} \text{cm}^{-3}$, $T_{\text{gas}} = 21 \text{K}$, the ionizing degree $y(e) = 3.7 \times 10^{-4}$ and the H_2 fraction $y(\text{H}_2) = 2 \times 10^{-6}$, reflecting the condition of the universe at $z = 16$ (Omukai et al. (2008)). It has been confirmed that the results are almost independent of the initial conditions as long as realistic values are chosen (Omukai et al. (2008)).

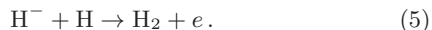
2.2 The effects of external radiation on the H_2 abundance

In this section, we briefly review the key processes determining the H_2 abundance under the influence of external radiation (for more detailed review, see e.g. O01). As explained in the introduction, primordial-gas clouds collapse via atomic cooling in the case that strong external radiation suppresses H_2 cooling. In the followings, we review two H_2 formation and dissociation channels and three photodissociation processes.

Let us start with reviewing the H_2 formation channel via intermediary H^- , which is the dominant H_2 formation channel in most cases. This channel begins with the H^- formation reaction,



which is followed by the H_2 formation reaction,



We denote the reaction rate coefficients for Eqs. (4) and (5) as $k_{\text{form}}^{(1)} [\text{cm}^3 \text{s}^{-1}]$ and $k_{\text{form}}^{(2)} [\text{cm}^3 \text{s}^{-1}]$, respectively. In the above chain, not all H^- molecules formed via Eq. (4) are

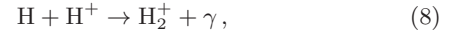
used for H_2 formation but some of them go back to H by the H^- photodissociation reaction,



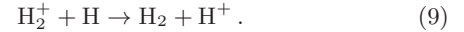
Here, the photodissociation rate coefficient, denoted as $k_{\text{H}^-, \text{pd}} [\text{s}^{-1}]$, is proportional to the number density of photons of external radiation. The rates of competing reactions given by Eqs. (5) and (6) determine the branching ratio of formed H^- to be used for H_2 formation. Since the reactions of Eqs. (5) and (6) proceeds much faster than that of Eq. (4), the formation rate of H_2 per unit volume per unit time can be written as $k_{\text{form}}^{(\text{eff})} n(\text{H}) n(e)$, where the effective H_2 formation rate coefficient $k_{\text{form}}^{(\text{eff})} [\text{cm}^3 \text{s}^{-1}]$ is given by

$$k_{\text{form}}^{(\text{eff})} \equiv k_{\text{form}}^{(1)} \left[\frac{k_{\text{form}}^{(2)} n(\text{H})}{k_{\text{form}}^{(2)} n(\text{H}) + k_{\text{H}^-, \text{pd}}} \right]. \quad (7)$$

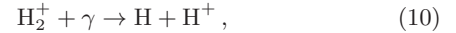
Next, we would like to review another H_2 formation channel via intermediary H_2^+ , which is less effective than the H_2 formation channel via H^- in most cases. This channel begins with the H_2^+ formation reaction,



which is followed by the H_2 formation reaction,

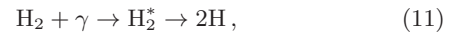


This channel can be regarded as an analogue of the H_2 formation channel via H^- . In this case, however, the reaction chain begins with collision of H with H^+ instead of e . In a similar way to the H_2 formation channel via H^- , not all the H_2^+ molecules formed via Eq. (8) are used for H_2 formation due to the H_2^+ photodissociation reaction,



where the photodissociation rate coefficient $k_{\text{H}_2^+, \text{pd}} [\text{s}^{-1}]$ is proportional to the density of photons of external radiation. Here, again, the rates of competing reactions given by Eqs. (9) and (10) determine the branching ratio of formed H_2^+ to be used for H_2 formation. In principle, the H_2 formation channel via H_2^+ can overwhelm that via H^- by suppressing only latter by H^- photodissociation. However, it is unlikely to be realized in our calculations since the strength of H_2^+ and H^- photodissociation are closely related, as explained in the last part of this section.

The main H_2 dissociation channel changes depending on the density of gas n . When n is small, the dominant channel is the H_2 photodissociation reaction,



where the H_2 photodissociation rate coefficient $k_{\text{H}_2, \text{pd}} [\text{s}^{-1}]$ is proportional to the density of photons of external radiation. On the other hand, when n is large, the dominant channel is the collisional dissociation reaction,



where we denote the collisional dissociation rate coefficient as $k_{\text{cd}, \text{H}_2} [\text{cm}^3 \text{s}^{-1}]$.

In the followings, we review the three photodissociation processes due to external radiation: H_2 , H^- and H_2^+ photodissociation.

First, let us review H_2 photodissociation given by Eq. (11). H_2 photodissociation is one of the key processes

in our calculations because it suppresses the H_2 abundance by directly dissociating H_2 molecules. The photodissociation rate coefficient $k_{\text{H}_2, \text{pd}}$ can be calculated from external radiation $J(\nu)$ as (Draine & Bertoldi (1996))

$$k_{\text{H}_2, \text{pd}} \approx \kappa_{\text{H}_2, \text{pd}} J_{\text{LW}}, \quad (13)$$

with $\kappa_{\text{H}_2, \text{pd}} = 1.4 \times 10^9$ (in cgs unit). Here, $\kappa_{\text{H}_2, \text{pd}}$ is estimated with $J_{\text{LW}} \equiv J(h\nu = 12.4 \text{ eV})$, the specific intensity at the center of LW bands ($11.2 \text{ eV} < h\nu < 13.6 \text{ eV}$), as shown in Fig. 1. The error due to estimating $k_{\text{H}_2, \text{pd}}$ by using the specific intensity at one frequency is usually negligible since $J(\nu)$ does not change significantly in the narrow frequency range of the LW bands.

The intensity in the LW bands is self-shielded by H_2 molecules when the H_2 column density of the central core N_{H_2} becomes large. We take this effect into account in our one-zone model by multiplying the intensity in the LW bands by a self-shielding factor f_{sh} . It seems that there is no complete agreement on the form of f_{sh} yet (see WG11 and Richings et al. (2014) hereafter R14), although, in principle, it should be determined uniquely by studying the effective amount of self-shielding with level-by-level radiative transfer calculations. Considering such situation, we decide to use the form of f_{sh} derived in WG11 as a fiducial model, but to study the influence of using different forms in Sec. 3.2.1. The form of f_{sh} derived in WG11 is

$$f_{\text{sh}}(N_{\text{H}_2}, T_{\text{gas}}) = \frac{0.965}{(1 + x/b_5)^{1.1}} + \frac{0.035}{(1 + x)^{0.5}} \times \exp[-8.5 \times 10^{-4}(1 + x)^{0.5}]. \quad (14)$$

where

$$x \equiv \frac{N_{\text{H}_2}}{5 \times 10^{14} \text{ cm}^{-2}}, \quad b_5 \equiv \frac{\sqrt{2kT_{\text{gas}}/2m_{\text{H}}}}{10^5 \text{ cm s}^{-1}}. \quad (15)$$

We assume N_{H_2} is given by

$$N_{\text{H}_2} = n(\text{H}_2) \lambda_{\text{J}}, \quad (16)$$

with the Jeans length λ_{J} given by Eq. (2).

Second, let us review H^- photodissociation given by Eq. (6). H^- photodissociation is also one of the key processes in our calculations because it suppresses the dominant H_2 formation channel by dissociating intermediary H^- . The photodissociation rate coefficient $k_{\text{H}^-, \text{pd}}$ is calculated from $J(\nu)$ as

$$k_{\text{H}^-, \text{pd}} = \int_0^\infty \frac{4\pi J(\nu)}{h\nu} \sigma_{\text{H}^-}(\nu) d\nu, \quad (17)$$

with the cross section $\sigma_{\text{H}^-}(\nu)$ of John (1988). We need to evaluate the frequency integral in Eq. (17) to obtain $k_{\text{H}^-, \text{pd}}$, since H^- photodissociation is caused by a wide range of photons ($0.76 \text{ eV} < h\nu$), as shown in Fig. 1. For later convenience, however, we introduce a similar expression to Eq. (13),

$$k_{\text{H}^-, \text{pd}} \approx \kappa_{\text{H}^-, \text{pd}} J_{2\text{eV}}, \quad (18)$$

where $J_{2\text{eV}} \equiv J(h\nu = 2.0 \text{ eV})$ and the information of the spectral shape of external radiation is contained in $\kappa_{\text{H}^-, \text{pd}}$. We note that $h\nu = 2.0 \text{ eV}$ is the frequency above and below which the integration in Eq. (17) is equal for a flat spectrum ($J(\nu) = \text{const.}$).

Finally, let us comment on H_2^+ photodissociation given by Eq. (10). The H_2^+ channel of the H_2 formation may

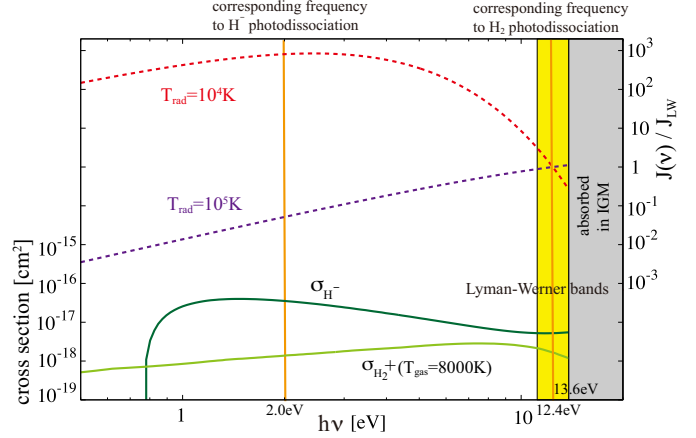


Figure 1. The cross sections for H^- photodissociation σ_{H^-} (green) and for H_2^+ photodissociation when $T_{\text{gas}} = 8000 \text{ K}$ $\sigma_{\text{H}_2^+}(T_{\text{gas}} = 8000 \text{ K})$ (light-green) are plotted. The LW bands, corresponding to H_2 photodissociation, are drawn as a yellow band. The black-body spectra $J(\nu)$ with $T_{\text{rad}} = 10^4 \text{ K}$ and 10^5 K are also plotted in the same figure. In this paper, we assume ionizing photons ($h\nu > 13.6 \text{ eV}$) are totally absorbed in the intergalactic medium (IGM). The specific intensities at $h\nu = 12.4 \text{ eV}$ and 2.0 eV are related to H_2 and H^- photodissociation, respectively (see Eqs. (13) and (18), respectively). The form of $\sigma_{\text{H}^-}(\nu)$ given by John (1988) can be used only for $h\nu < 9.8 \text{ eV}$, but we keep using it even for $h\nu > 9.8 \text{ eV}$ since the error introduced by this treatment is expected to be negligibly small.

become the dominant channel when H^- photodissociation suppresses the H^- channel, which is dominant without any photodissociation. In the followings, we check which channel is dominant, in the case that the H_2^+ channel, as well as the H^- channel, is suppressed by photodissociation. We use the cross section $\sigma_{\text{H}_2^+}(\nu, T_{\text{gas}})$ given by Stancil (1994) ($T_{\text{gas}} > 2000 \text{ K}$) and Mihajlov et al. (2007) ($T_{\text{gas}} < 2000 \text{ K}$). The cross section $\sigma_{\text{H}_2^+}$ depends on T_{gas} because H_2^+ is easier to be dissociated from excited states, which are assumed to be populated according to the LTE distribution with T_{gas} . In the case that $T_{\text{gas}} \sim 8000 \text{ K}$, the frequency range contributing to H_2^+ photodissociation is wider than that contributing to H^- photodissociation, while $\sigma_{\text{H}_2^+}$ is smaller than σ_{H^-} by an order of magnitude at $h\nu > 0.76 \text{ eV}$, as shown in Fig. 1, and thus the frequency integrated H_2^+ photodissociation rate coefficient $k_{\text{H}_2^+, \text{pd}}$, defined in a similar way to Eq. (17), becomes also large in the case $k_{\text{H}^-, \text{pd}}$ is large. Therefore, the H_2^+ channel is always subdominant even if the photodissociation processes are considered.

3 RESULTS

3.1 The evolution of primordial-gas clouds under external radiation

In this section, we review physical processes proceeding during the gravitational collapse of primordial-gas clouds under external radiation, showing several results of our one-zone calculations. Following the argument in O01, we see how the evolutionary trajectories bifurcate to the atomic and H_2 cooling tracks depending on the strength and spectral

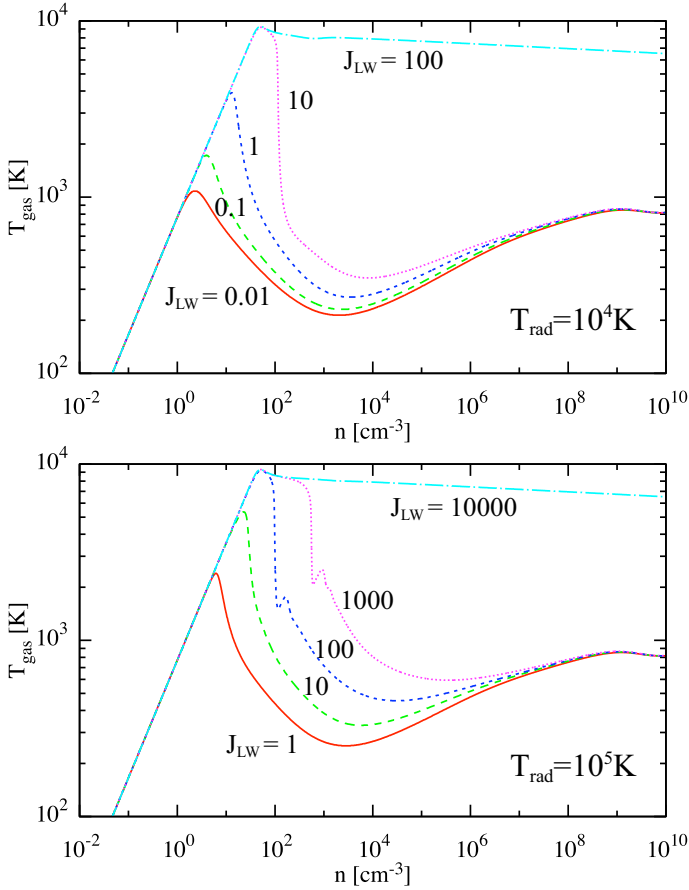


Figure 2. Density-temperature relation for the collapse of primordial-gas clouds under radiation with the black-body spectra with $T_{\text{rad}} = 10^4$ K (top panel) and 10^5 K (bottom panel). We take the specific intensity at the LW bands as $J_{\text{LW}} = 0.01, 0.1, 1, 10, 100$ and $J_{\text{LW}} = 1, 10, 100, 1000, 10000$ for the $T_{\text{rad}} = 10^4$ K and 10^5 K cases, respectively.

shape of external radiation. We make calculations of collapsing clouds irradiated by the black-body spectra with $T_{\text{rad}} = 10^4$ K and $T_{\text{rad}} = 10^5$ K. We specify the strength of radiation using $J_{\text{LW}, 21}$, in units of $10^{-21} \text{ erg s}^{-1} \text{ Hz}^{-1} \text{ sr}^{-1} \text{ cm}^{-2}$.

The results are shown in Figs. 2, where it can be clearly seen that the evolutionary trajectories bifurcate to one of two types of tracks: the atomic and H_2 cooling tracks. In the case that the atomic cooling track is chosen, the clouds evolve almost isothermally with $T_{\text{gas}} \sim 8000$ K by atomic cooling. On the other hand, in the case that the H_2 cooling track is chosen, the evolutionary trajectories rapidly merge to the H_2 cooling track when H_2 cooling becomes effective and the clouds cool down to $T_{\text{gas}} \lesssim 1000$ K. By increasing external radiation, the trajectories get closer to the atomic cooling track, and finally merge to the atomic cooling track at $J_{\text{LW}, 21} = 100$ and 10000 for $T_{\text{rad}} = 10^4$ K and 10^5 K, respectively. The atomic cooling track is chosen in the case that H_2 molecules needed for H_2 cooling are suppressed by the strong external radiation.

The conditions of the gas when n is close to the critical density n_{cr} is crucial in determining which track is finally chosen (OO1). Here, n_{cr} is defined as the density above which the population of the internal states of H_2 is determined by the LTE distribution due to sufficient collisional

excitation. For both vibrational and rotational excitations of H_2 molecules, n_{cr} is about 10^3 cm^{-3} for $T_{\text{gas}} \sim 8000$ K. The former and latter excitations are closely related to the collisional dissociation and cooling processes, respectively. When $n > n_{\text{cr}}$, H_2 molecules are easily dissociated via collisional dissociation and, in addition, cooling rate per H_2 molecule saturates and H_2 cooling becomes less effective than compressional heating. On the other hand, the H_2 formation channel given by Eqs. (4) and (5) becomes effective as n increases. Thus, although H_2 becomes easier to be formed as n increases until n_{cr} , once a trajectory passes through n_{cr} , it is difficult to make transition from the atomic cooling track to the H_2 cooling track. Therefore, the fate of a trajectory can be known by examining whether the sufficient amount of H_2 molecules is formed around $n \sim n_{\text{cr}}$. Once H_2 molecules are formed and H_2 cooling becomes effective, collisional dissociation is suppressed due to the decrease of T_{gas} and, in addition, H_2 photodissociation is suppressed due to the self-shielding of the LW photons by H_2 molecules, and thus the trajectory rapidly converges to the H_2 cooling track.

Let us see how the abundance of H_2 is determined when the formation and dissociation processes balance each other under external radiation. If the specific intensity of external radiation is about that needed for the atomic cooling track, H_2 photodissociation is the main dissociation process around $n \sim n_{\text{cr}}$ (OO1; S10). Thus, by equating the H_2 formation rate of the channel given by Eqs. (4) and (5) and the H_2 dissociation rate of the photodissociation process given by Eq. (11), we obtain $k_{\text{form}}^{(\text{eff})} n(\text{H}) n(e) = k_{\text{H}_2, \text{pd}} n(\text{H}_2)$. By using this equation and Eqs. (7), (13) and (18) and assuming $n(\text{H}) \approx n$, we obtain

$$y(\text{H}_2) = \left[\frac{k_{\text{form}}^{(1)}}{\kappa_{\text{H}_2, \text{pd}} J_{\text{LW}}} \right] \left[\frac{k_{\text{form}}^{(2)} n}{k_{\text{form}}^{(2)} n + \kappa_{\text{H}^-, \text{pd}} J_{2\text{eV}}} \right] n y(e). \quad (19)$$

From this equation, it is clear that $y(\text{H}_2)$ becomes small if the first square bracket is suppressed due to large $\kappa_{\text{H}_2, \text{pd}} J_{\text{LW}}$ and/or the second is suppressed due to large $\kappa_{\text{H}^-, \text{pd}} J_{2\text{eV}}$. In other words, the amount of H_2 can be suppressed by strong H_2 and/or H^- photodissociation.

Equation (19) helps us to physically understand the T_{rad} and J_{LW} dependence of the evolution. To begin with, we explain why the clouds under the radiation with the same $J_{\text{LW}} = 100$ evolve along the atomic cooling track in the case $T_{\text{rad}} = 10^4$ K but along the H_2 cooling track in the case $T_{\text{rad}} = 10^5$ K. In the $T_{\text{rad}} = 10^4$ K case, we obtain $k_{\text{H}^-, \text{pd}} \sim 5 \times 10^{-6} \text{ s}^{-1}$ with Eq. (17) and $k_{\text{form}}^{(2)} n_{\text{cr}} \sim 1 \times 10^{-6} \text{ s}^{-1}$ with $n_{\text{cr}} \sim 10^3 \text{ cm}^{-3}$ and $k_{\text{form}}^{(2)} = 1.3 \times 10^{-9} \text{ cm}^3 \text{ s}^{-1}$ (Glover & Abel (2008)). Thus, the second square bracket of Eq. (19) is significantly smaller than 1, meaning H^- photodissociation plays a role in suppressing H_2 formation. On the other hand, in the $T_{\text{rad}} = 10^5$ K case, $k_{\text{H}^-, \text{pd}} \sim 1 \times 10^{-9}$ and the second square bracket of Eq. (19) is almost 1, meaning the effect of H^- photodissociation is negligible. Therefore, the two clouds with different T_{rad} evolve along different tracks although the strength of H_2 photodissociation is same due to the same J_{LW} .

Next, we explain why the clouds under the radiation with same $T_{\text{rad}} = 10^5$ K evolve along the atomic cooling track in the case $J_{\text{LW}} \leq 1000$ but along the H_2 cooling track in the case $J_{\text{LW}} = 10000$. Even in the case $J_{\text{LW}} = 10000$, the

second square-bracket of Eq. (19) is almost 1 and the effect of H^- photodissociation is negligible. In the case $J_{\text{LW}} = 10000$, however, H_2 photodissociation is very strong and the first square-bracket of Eq. (19) becomes very small. Therefore, the cloud under the radiation with $T_{\text{rad}} = 10^5$ K and $J_{\text{LW}} = 10000$ evolves along the atomic cooling track by suppressing the H_2 abundance with strong H_2 photodissociation without any help of H^- photodissociation.

3.2 J^{crit} for black-body spectra

In this section, we present J^{crit} for the black-body spectra with temperatures $7000 \text{ K} < T_{\text{rad}} < 200000 \text{ K}$, to understand the dependence of J^{crit} on the hardness of the spectrum of external radiation. We calculate J^{crit} with different forms of self-shielding factors because there is some disagreement on the form of self-shielding factor, as mentioned in Sec. 2.2. We also make comparison of our results with the literature (S10 and WG11). In practice, J^{crit} is calculated with the bisection method by examining whether T_{gas} is larger or smaller than 4000 K at $n = 10^7 \text{ cm}^{-3}$. In this section, we use both J_{LW} and J_{Lyc} to specify the strength of radiation, in order to make it easier to compare our result with the literature (J_{Lyc} was used in, e.g., O01, S10, WG11). Note that we mainly use J_{LW} other than this section because the specific intensity at the LW bands is more directly related to the physics we are interested in.

The results for our fiducial model, in which the self-shielding factor of WG11 is used, are shown as the red lines in Fig. 3. As T_{rad} increases, J^{crit} becomes larger: $J_{21, \text{LW}}^{\text{crit}} = 60$ at $T_{\text{rad}} = 10^4 \text{ K}$, $J_{21, \text{LW}}^{\text{crit}} = 1200$ at $T_{\text{rad}} = 2 \times 10^4 \text{ K}$. However, the T_{rad} dependence of $J_{21, \text{LW}}^{\text{crit}}$ becomes very weak for the case $T_{\text{rad}} \gtrsim 3 \times 10^4 \text{ K}$, for which $J_{21, \text{LW}}^{\text{crit}} \sim 1400$ and is almost constant.

The T_{rad} dependence of J^{crit} can be understood with Eq. (19) in a similar manner to that in Sec. 3.1. As T_{rad} decreases J^{crit} becomes smaller because H^- photodissociation suppress H_2 formation more effectively (the second square-bracket of Eq. (19) becomes smaller). For high T_{rad} ($T_{\text{rad}} \gtrsim 3 \times 10^4 \text{ K}$), the dependence of $J_{21, \text{LW}}^{\text{crit}}$ on T_{rad} is weak, because the effect of H^- photodissociation is negligibly small (the second square-bracket of Eq. (19) is almost unity).

3.2.1 Influence of using different self-shielding factors

In the followings, we discuss the influence of using different forms of self-shielding factors f_{sh} . The form of f_{sh} derived in Draine & Bertoldi (1996) (hereafter DB96) has been widely used in the literature (e.g. O01; S10). However, WG11 modified it to reproduce the results of their radiative transfer calculations with three-dimensional hydrodynamic simulations for gas with $T_{\text{gas}} \sim 8000 \text{ K}$. Recently, R14 proposed another form of f_{sh} , arguing that the form derived in WG11 underestimates the strength of self-shielding compared with their radiative transfer calculations with CLOUDY (Ferland et al. (1998)).

In this section, we introduce the three different forms of f_{sh} . First, the form of f_{sh} derived in WG11 is given by

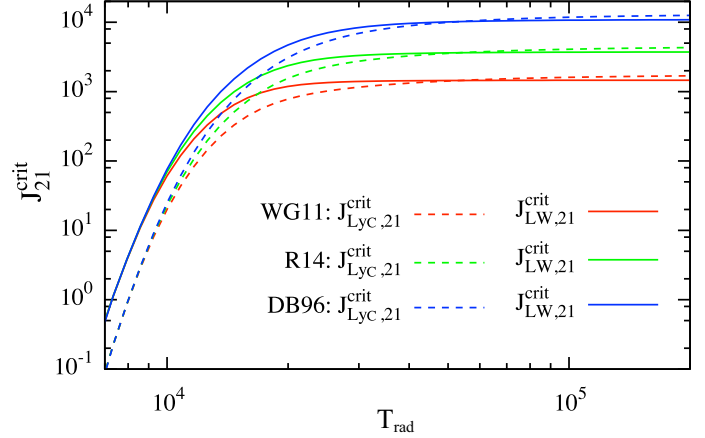


Figure 3. The critical radiation intensity J^{crit} for the black-body spectra with T_{rad} . The critical LW intensity $J_{\text{LW}, 21}^{\text{crit}}$ and the critical Lyc intensity $J_{\text{Lyc}, 21}^{\text{crit}}$ are plotted as solid and dashed lines, respectively. The red, green and blue lines are the results with the self-shielding factors of WG11, R14 and DB96, respectively.

Eq. (14). Second, the form derived in DB96 is given by

$$f_{\text{sh}}(N_{\text{H}_2}) = \min \left[1, \left(\frac{N_{\text{H}_2}}{10^{14} \text{ cm}^{-2}} \right)^{-3/4} \right]. \quad (20)$$

Third, the form derived in R14 is given by

$$f_{\text{sh}}(N_{\text{H}_2}, T_{\text{gas}}) = \frac{1 - \omega_{\text{H}_2}(T_{\text{gas}})}{(1 + x'/b_5)^{\alpha(T_{\text{gas}})}} \exp[-5 \times 10^{-7}(1 + x')] + \frac{\omega_{\text{H}_2}(T_{\text{gas}})}{(1 + x')^{0.5}} \exp[-8.5 \times 10^{-4}(1 + x')^{0.5}], \quad (21)$$

where

$$x' \equiv \frac{N_{\text{H}_2}}{N_{\text{crit}}(T_{\text{gas}})}, \quad (22)$$

$$\frac{N_{\text{crit}}(T_{\text{gas}})}{10^{14} \text{ cm}^{-2}} = \begin{cases} 1.3 \left[1 + \left(\frac{T_{\text{gas}}}{600 \text{ K}} \right)^{0.8} \right] & T_{\text{gas}} < 3000 \text{ K} \\ \left(\frac{T_{\text{gas}}}{4760 \text{ K}} \right)^{-3.8} & 3000 \text{ K} \leq T_{\text{gas}} < 4000 \text{ K} \\ 2.0 & 4000 \text{ K} \leq T_{\text{gas}} \end{cases}, \quad (23)$$

$$\omega_{\text{H}_2}(T_{\text{gas}}) = 0.013 \left[1 + \left(\frac{T_{\text{gas}}}{2700 \text{ K}} \right)^{1.3} \right]^{\frac{1}{1.3}} \exp \left[- \left(\frac{T_{\text{gas}}}{3900 \text{ K}} \right)^{14.6} \right], \quad (24)$$

and

$$\alpha(T_{\text{gas}}) = \begin{cases} 1.4 & T_{\text{gas}} < 3000 \text{ K} \\ \left(\frac{T_{\text{gas}}}{4500 \text{ K}} \right)^{-0.8} & 3000 \text{ K} \leq T_{\text{gas}} < 4000 \text{ K} \\ 1.1 & 4000 \text{ K} \leq T_{\text{gas}} \end{cases}. \quad (25)$$

We present in Fig. 3 the critical intensity J^{crit} for the black-body radiation with T_{rad} for the three forms of f_{sh} given above. Difference in f_{sh} affects J^{crit} more for higher T_{rad} . For instance, for the $T_{\text{rad}} = 10^4 \text{ K}$ cases, in which H^- photodissociation plays a key role in suppressing the H_2 formation independently of self-shielding, J^{crit} is almost same

Table 1. Galaxy/IGM models explored

IMF	Salpeter IMF with 1-100 M_{\odot} (fixed)
metallicity (Z/Z_{\odot})	0 (Pop III), 5×10^{-4} , 0.02, 0.2
SF type: Age	instantaneous starburst (IS): 1 Myr, 10 Myr, 100 Myr-1 Gyr* constant star formation (CS): 1 Myr, 10 Myr, 100 Myr, 500 Myr
escape fraction (f_{esc})	0, 0.5
IGM absorption ($\text{Ly}\alpha$)	complete/no absorption
IGM absorption ($>\text{Ly}\alpha$)	complete absorption (fixed)

* IS galaxies with age between 100 Myr and 1 Gyr are studied with the bin width of 0.1 on a logarithmic scale.

for all three cases. On the other hand, for the $T_{\text{rad}} = 10^5$ K cases, in which the evolutionary trajectories are totally determined by the strength of H_2 photodissociation, difference in f_{sh} affects significantly and $J_{21, \text{LW}}^{\text{crit}} = 1500, 3700$ and 11000 with f_{sh} of WG11, R14 and DB96, respectively. In summary, the influence of using different forms of f_{sh} is not negligible.

Before ending this section, we make comparison of our results with the literature (S10 and WG11). S10 used f_{sh} of DB96 to obtain $J_{21, \text{Lyc}}^{\text{crit}} = 39$ and 12000 for $T_{\text{rad}} = 10^4$ K and 10^5 K, respectively. Our results with the same f_{sh} are $J_{21, \text{Lyc}}^{\text{crit}} = 25$ and 14000 for $T_{\text{rad}} = 10^4$ K and 10^5 K, respectively. WG11 used their own f_{sh} to obtain $J_{21, \text{Lyc}}^{\text{crit}} = 1400$ for the black-body spectrum with $T_{\text{rad}} = 10^5$ K. Our result with the same f_{sh} is $J_{21, \text{Lyc}}^{\text{crit}} = 1600$ for $T_{\text{rad}} = 10^4$ K. In general, our results are in good agreement with those obtained in S10 and WG11. The remaining differences might be due to the use of different chemical reaction rates and cooling functions, because we use those of Glover & Abel (2008) while S10 and WG11 used those of Galli & Palla (1998).

3.3 J^{crit} for realistic spectra

In this section, we present J^{crit} for realistic spectra considering various models of source galaxies and IGM radiative transfer. It is needed to obtain J^{crit} for each realistic spectrum, because realistic spectra in general do not look like the black-body spectra and cannot be parameterized with a single parameter like T_{rad} . To obtain the spectra of galaxies, we adopt the spectral model by Inoue (2011), who added nebular lines and continua to the stellar population synthesis models of Schaerer (2003) for $Z/Z_{\odot} = 0$ (Pop III) and $Z/Z_{\odot} = 5 \times 10^{-4}$ and of STARBURST99 (Leitherer et al. (1999)) for $Z/Z_{\odot} = 0.02$ and $Z/Z_{\odot} = 0.2$ by a metallicity dependent way.

The models of galaxies and IGM radiative transfer explored in this paper are summarized in Table 1. Since we are interested in the early universe, we focus on metal-poor galaxies with $Z/Z_{\odot} = 0$ (Pop III), 5×10^{-4} , 0.02 and 0.2, where the solar metallicity $Z_{\odot} = 0.02$. We assume a Salpeter type initial mass function (IMF) with the stellar mass range 1 – 100 M_{\odot} . We consider two types of star formation (SF) histories: instantaneous starburst (IS) and constant star formation (CS). For the CS galaxies we assume the duration of star formation is 1 Myr, 10 Myr, 100 Myr and 500 Myr,

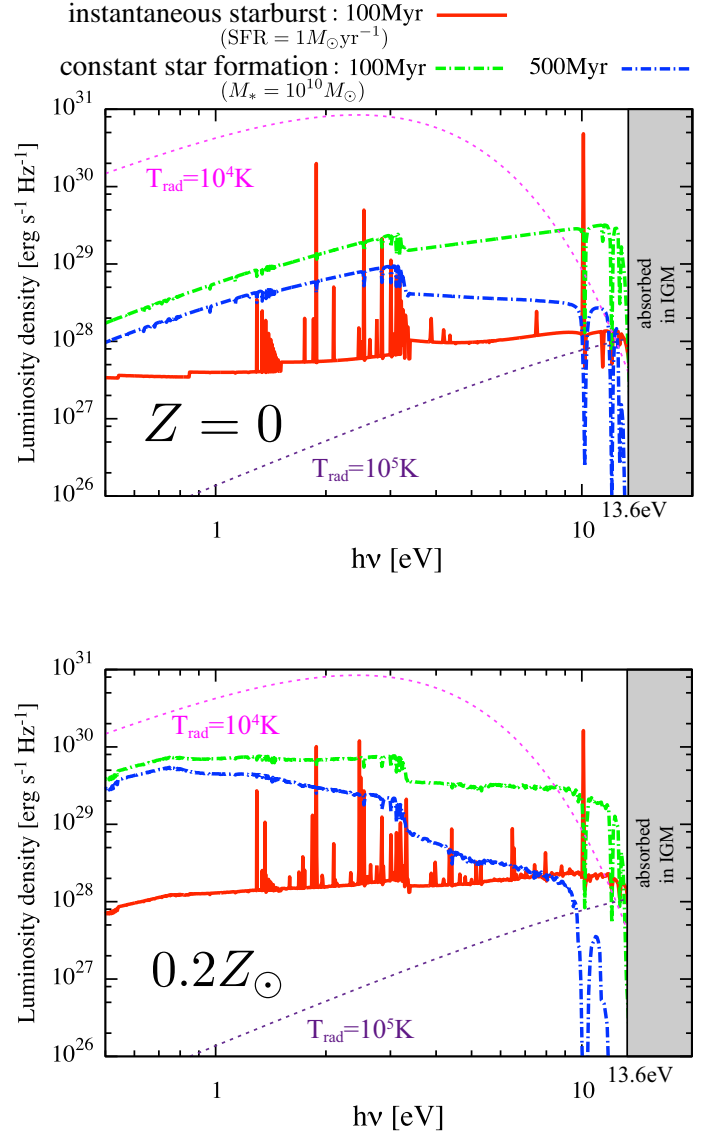


Figure 4. The spectra of galaxies with metallicity $Z = 0$ (Pop III) (top panel) and $Z/Z_{\odot} = 0.2$ (bottom panel). For both cases, we take $f_{\text{esc}} = 0$ and plot the spectra of the constant star formation galaxies with a duration of star formation 100 Myr (with the star formation rate (SFR) = $1 M_{\odot} \text{yr}^{-1}$) and the instantaneous starburst galaxies with a time since the burst 100 Myr and 500 Myr (with the total stellar mass $M_{\ast} = 10^{10} M_{\odot}$). We do not consider $\text{Ly}\alpha$ absorption by the IGM in this figure. The emission-line width is assumed to be 300 km s^{-1} for illustrating purposes. For comparison, we also plot the black-body spectra with $T_{\text{rad}} = 10^4$ K and 10^5 K arbitrary scaled in the panels.

while for the IS galaxies we assume the time since the burst is 1 Myr, 10 Myr and between 100 Myr and 1 Gyr with the bin width of 0.1 on a logarithmic scale. We consider the two cases for the escape fraction of ionizing photons from source galaxies f_{esc} and take $f_{\text{esc}} = 0$ and 0.5, where the absorbed energies of the ionizing photons are converted to the nebular emission. We assume that all ionizing photons from galaxies are absorbed by the intergalactic medium (IGM), but consider the two cases for the $\text{Ly}\alpha$ line, where it is either completely absorbed by the IGM or not at all. As a whole, we explore $4 \times 4 \times 2 \times 2 = 64$ and $4 \times 13 \times 2 \times 2 = 208$ models of

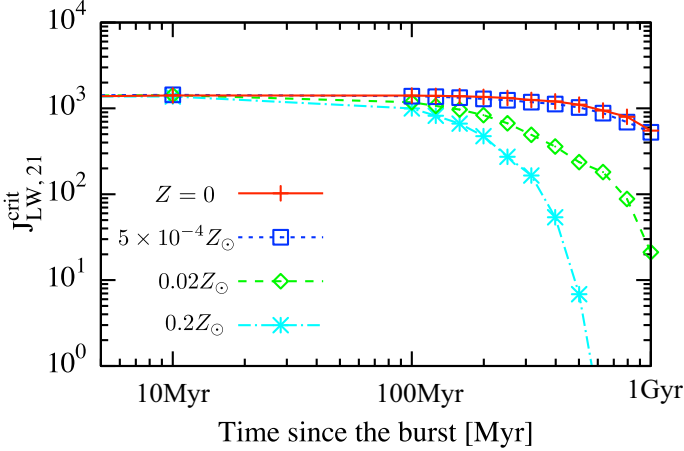


Figure 5. The critical LW intensity $J_{LW,21}^{crit}$ for realistic spectra of the IS galaxies with $Z = 0$, $5 \times 10^{-4} Z_{\odot}$, $0.02 Z_{\odot}$ and $0.2 Z_{\odot}$. We assume complete Ly α absorption and $f_{esc} = 0$. The horizontal axis is the time since the burst. $J_{LW,21}^{crit} \sim 1400$ at 1 Myr since the burst irrespective of metallicity. In the case of the CS galaxies, $J_{LW,21}^{crit} = 1300 - 1400$ irrespective of the metallicity and the duration of SF.

the IS and CS galaxies, respectively. It should be noted that old galaxies studied in this section are not proper candidates for sources of radiation contributing to DCBH formation at $z \gtrsim 10$, since the age of the universe is about 500 Myr at $z = 10$. However, we explore a wide range of galaxies to see the dependence of J^{crit} on spectra clearly.

As examples, we show the spectra of the $Z = 0$ (Pop III) and $Z/Z_{\odot} = 0.2$ galaxies in Figs. 4. The spectra are roughly flat in the frequency range $h\nu \lesssim 10$ eV due to the superposition of the stellar emission with various effective temperatures. The number of the LW photons from the old IS galaxies is exponentially suppressed, because the high temperature stars that contribute to producing the LW photons no longer emit radiation in such galaxies due to their short lifetimes.

The results of J^{crit} for realistic spectra are summarized as follows. While $J_{LW,21}^{crit} = 1300 - 1400$ for all CS galaxies irrespective of the metallicity and duration of SF, J^{crit} has a wide range of values for the IS galaxies depending on the models, as shown in Fig. 5. We plot only the cases of complete Ly α absorption and $f_{esc} = 0$ in Fig. 5, because the effects of changing Ly α absorption and f_{esc} make at most 5% difference to the values of J^{crit} although the Ly α line and the nebular emission contribute to H $^{-}$ photodissociation and slightly reduce the value of J^{crit} . The critical intensity J^{crit} decreases as the IS galaxies become older or more metal-enriched, although the dependence is weak for the young or extremely metal-poor galaxies. For the young galaxies with the time since burst less than 100 Myr $J_{LW,21}^{crit} = 1000 - 1400$, while for the extremely metal-poor and not very old galaxies ($Z \leq 5 \times 10^{-4} Z_{\odot}$ and the time since burst is less than 500 Myr) $J_{LW,21}^{crit} \approx 1400$ and is almost constant.

3.4 The reason for the dependence of J^{crit} on spectra

In this section, we explain the reason for the dependence of J^{crit} on the spectral shape of external radiation, as seen

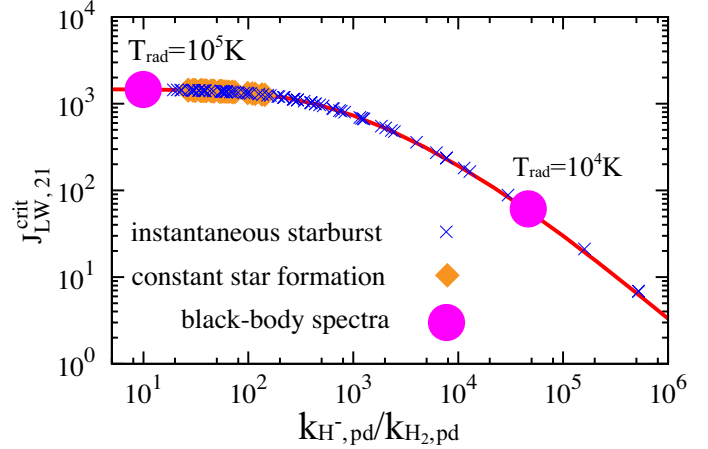


Figure 6. The critical LW intensity $J_{LW,21}^{crit}$ with respect to $k_{H-,pd}/k_{H2,pd}$ for the realistic spectra (blue points and orange diamonds corresponding to IS and CS galaxies, respectively) and black-body spectra with $T_{rad} = 10^4$ K and 10^5 K (magenta dots). The value of $k_{H-,pd}/k_{H2,pd}$ represents the hardness of each spectrum. We also plot $J_{LW,21}^{crit}$ with respect to $k_{H-,pd}/k_{H2,pd}$ obtained by assuming $k_{H2+,pd}/k_{H-,pd} = 0.1$ (red line).

in Sec. 3.2 and Sec. 3.3, by pointing out the key parameter determining J^{crit} . We then develop a method to estimate J^{crit} for a given spectrum without calculating the evolution of the clouds.

3.4.1 The key parameter determining J^{crit}

In this section, we propose a hypothesis that the ratio of the H $^{-}$ and H $_2$ photodissociation rates, $k_{H-,pd}/k_{H2,pd}$, is the key parameter determining the dependence of J^{crit} on spectra, and prove its validity in the followings. We come up with this hypothesis because, as explained in Sec. 3.1, in the cases strong H $^{-}$ photodissociation suppresses H $_2$ formation, smaller J_{LW} (and hence weaker H $_2$ photodissociation) is needed to suppress H $_2$ cooling. In this section, the quantity written as $k_{H2,pd}$ is not the true value realized in clouds during the evolution but that defined by Eq. (13) without considering the effect of self-shielding. Here, we are interested in the quantity directly related to external radiation.

To demonstrate that $k_{H-,pd}/k_{H2,pd}$ is the only parameter determining J^{crit} , we obtain $k_{H-,pd}/k_{H2,pd}$ for the realistic and black-body spectra studied in this paper and plot them with J^{crit} in Fig. 6. It is clear from Fig. 6 that there is one-to-one correspondence between $k_{H-,pd}/k_{H2,pd}$ and J^{crit} . In other words, J^{crit} is solely determined by $k_{H-,pd}/k_{H2,pd}$. We plot only the results for the complete Ly α absorption and $f_{esc} = 0$ cases in Fig. 6, because the effects of changing Ly α absorption and f_{esc} make little difference. The $k_{H-,pd}/k_{H2,pd}$ dependence of J^{crit} can be understood with Eq. (19), in the same manner as the T_{rad} dependence (see the last part of Sec. 3.2).

Note that $k_{H-,pd}/k_{H2,pd}$ can be regarded as a proxy for the hardness of the spectrum. The relation between T_{rad} and $k_{H-,pd}/k_{H2,pd}$ are given in Table 2. The ratio $k_{H-,pd}/k_{H2,pd}$ increases as T_{rad} decreases, corresponding to the fact that H $^{-}$ photodissociation becomes more effective as the spectrum becomes soft. The dependence of

Table 2. The relation between T_{rad} and $k_{\text{H}^-, \text{pd}}/k_{\text{H}_2, \text{pd}}$.

T_{rad} [K]	8×10^3	1×10^4	2×10^4	3×10^4	5×10^4	1×10^5	2×10^5
$k_{\text{H}^-, \text{pd}}/k_{\text{H}_2, \text{pd}}$	8.7×10^5	4.6×10^4	2.1×10^2	4.6×10^1	1.7×10^1	1.0×10^1	8.1×10^0

Table 3. The values of $\alpha_{\text{H}^-, \text{pd}}$ for the power-law spectra $J(\nu) \propto \nu^s$

s	-2	-1.5	-1	-0.5	0	0.5	1	1.5	2
$\alpha_{\text{H}^-, \text{pd}}$	1.44	1.21	1.06	0.99	1.00	1.12	1.41	2.03	3.32

$k_{\text{H}^-, \text{pd}}/k_{\text{H}_2, \text{pd}}$ on T_{rad} becomes weak for high T_{rad} ($\gtrsim 5 \times 10^5$ K). This is because for such high T_{rad} the spectrum obeys the Rayleigh-Jeans law ($J(\nu) \propto \nu^2$) in the frequency range contributing to H^- and H_2 photodissociation ($0.76 \text{ eV} < h\nu < 13.6 \text{ eV}$).

By obtaining the relation between $k_{\text{H}^-, \text{pd}}/k_{\text{H}_2, \text{pd}}$ and J^{crit} in advance, J^{crit} for a given spectrum can be estimated from this relation without calculating the evolution of the clouds. However, there remains one uncertainty. In order to determine the evolution of clouds, the H_2^+ photodissociation rate should be specified in addition to J_{LW} (which determines $k_{\text{H}_2, \text{pd}}$ by Eq. (13)) and $k_{\text{H}^-, \text{pd}}/k_{\text{H}_2, \text{pd}}$. In the followings, we assume $k_{\text{H}_2^+, \text{pd}}/k_{\text{H}^-, \text{pd}} = 0.1$, motivated by the fact that $k_{\text{H}_2^+, \text{pd}}/k_{\text{H}^-, \text{pd}} \sim 0.1$ when $T_{\text{gas}} \sim 8000 \text{ K}$ during the evolution of the clouds under the external radiation with the realistic and thermal spectra. This assumption is further justified by the fact that the detailed value of $k_{\text{H}_2^+, \text{pd}}/k_{\text{H}^-, \text{pd}}$ is not important. We have also made calculations for the cases with $k_{\text{H}_2^+, \text{pd}}$ 10 times larger or smaller than the true values, but have found only negligible difference in the results. The relation between J^{crit} and $k_{\text{H}^-, \text{pd}}/k_{\text{H}_2, \text{pd}}$ obtained with the above assumption is shown as the red line in Fig. 6. For the realistic and thermal spectra studied in this paper, this relation almost perfectly reproduces the J^{crit} from the information of $k_{\text{H}^-, \text{pd}}/k_{\text{H}_2, \text{pd}}$.

For later convenience, we present a fitting formula to the relation given above,

$$J_{\text{LW}, 21}^{\text{crit}} = \begin{cases} 1400 & x \leq 0 \\ 1400 \times 10^{(a_1 x + a_2 x^2)} & x > 0 \end{cases}, \quad (26)$$

where

$$x = \log_{10} (k_{\text{H}^-, \text{pd}}/k_{\text{H}_2, \text{pd}}) - 2, \quad (27)$$

and

$$a_1 = -0.19, \quad a_2 = -0.12. \quad (28)$$

We find, for the realistic and black-body spectra studied in this paper, this fitting formula reproduces the J^{crit} from $k_{\text{H}^-, \text{pd}}/k_{\text{H}_2, \text{pd}}$ with at most 10% error in the range $1 < k_{\text{H}^-, \text{pd}}/k_{\text{H}_2, \text{pd}} < 10^5$. With this fitting formula, J^{crit} can be easily estimated from $k_{\text{H}^-, \text{pd}}/k_{\text{H}_2, \text{pd}}$ for a given spectrum.

3.4.2 A method to estimate J^{crit} for a given spectrum

Here, we propose a simple and easy method to estimate J^{crit} for a given spectrum. As mentioned in Sec. 3.4.1, the relation between $k_{\text{H}^-, \text{pd}}/k_{\text{H}_2, \text{pd}}$ and J^{crit} can be used to estimate J^{crit} . However, to use this relation, the frequency integral in Eq. (17) is needed to be evaluated in obtaining $k_{\text{H}^-, \text{pd}}$. The information of the spectral shape is contained in $\kappa_{\text{H}^-, \text{pd}}$ in Eq. (18), which can be parameterized with $\alpha_{\text{H}^-, \text{pd}}$ as

$$\kappa_{\text{H}^-, \text{pd}} = \alpha_{\text{H}^-, \text{pd}} \kappa_{\text{H}^-, \text{pd}}^{(0)}, \quad (29)$$

where $\kappa_{\text{H}^-, \text{pd}}^{(0)} = 1.1 \times 10^{11}$ (in cgs unit) is defined as $\kappa_{\text{H}^-, \text{pd}}$ for the flat spectrum ($J(\nu) = \text{const.}$). The values of $\alpha_{\text{H}^-, \text{pd}}$ for the power-law spectra $J(\nu) \propto \nu^s$ are given in Table 3. In the followings, we avoid the numerical integration of Eq. (17) by approximating $\kappa_{\text{H}^-, \text{pd}}$ with $\kappa_{\text{H}^-, \text{pd}}^{(0)}$. The realistic spectra are roughly flat in the frequency range $h\nu \lesssim 10 \text{ eV}$, as mentioned in Sec. 3.3, and thus the error due to this approximation can be estimated with the spread of $\alpha_{\text{H}^-, \text{pd}}$ around a flat spectrum and is expected to be small. By using this approximation with Eqs. (13) and (18), we can estimate $k_{\text{H}^-, \text{pd}}/k_{\text{H}_2, \text{pd}}$ from $J_{2\text{eV}}/J_{\text{LW}}$ simply as

$$k_{\text{H}^-, \text{pd}}/k_{\text{H}_2, \text{pd}} \approx 79 J_{2\text{eV}}/J_{\text{LW}}. \quad (30)$$

In the light of this relation, we modify the fitting formula given by Eqs. (26), (27) and (28) by redefining x in Eq. (27) as

$$x = \log_{10} (79 J_{2\text{eV}}/J_{\text{LW}}) - 2. \quad (31)$$

To check the validity of the formula given by Eqs. (26), (28) and (31), we obtain $J_{2\text{eV}}/J_{\text{LW}}$ for the realistic and black-body spectra studied in this paper and compare them with J^{crit} estimated from $J_{2\text{eV}}/J_{\text{LW}}$ with this formula. The result is that the formula reproduces J^{crit} with at most 30% error for both the realistic and black-body spectra. Although the error is larger than the formula given in Sec. 3.4.1, it is still practically negligible considering an order-of-magnitude scatter of J^{crit} due to the diversity in the three-dimensional structure of the clouds (S10; Latif et al. (2014)).

4 SUMMARY AND DISCUSSION

By using the one-zone model described in Sec. 2, we have calculated the critical intensity of external radiation needed

for primordial-gas clouds in halos with $T_{\text{vir}} \gtrsim 10^4$ K to form DCBHs by suppressing H_2 cooling. By performing series of calculations for various types of external radiation, we have examined the dependence of J^{crit} on the spectral shape of external radiation.

In Sec. 3.2, we have seen how J^{crit} changes depending on the temperature of the black-body spectra between $7000 \text{ K} < T_{\text{rad}} < 20000 \text{ K}$. In Sec. 3.3, we have determined J^{crit} for the realistic spectra of the metal-poor galaxies, by taking the data from the stellar population synthesis models. We have found J^{crit} is not sensitive to the age or metallicity for the constant star formation galaxies with $J_{\text{LW},21}^{\text{crit}} = 1300 - 1400$, while J^{crit} decreases as galaxies become older or more metal-enriched for the instantaneous starburst galaxies. However, such dependence for the instantaneous starburst galaxies is weak for the young or extremely metal-poor galaxies: $J_{\text{LW},21}^{\text{crit}} = 1000 - 1400$ for the young (the age less than 100 Myr) galaxies and $J_{\text{LW},21}^{\text{crit}} \approx 1400$ for the extremely metal-poor ($Z < 5 \times 10^{-4} Z_{\odot}$) and not very old (the age less than 500 Myr) galaxies. It should be noted that the above values of J^{crit} are obtained with f_{sh} of WG11 and that those obtained with f_{sh} of R14 are about two times larger than the above values, as shown in Sec. 3.2.1. It is important to precisely determine the form of f_{sh} but is beyond the scope of this work.

We have also found that the dependence of J^{crit} on the spectral shape is totally attributable to a single parameter $k_{\text{H}^-, \text{pd}}/k_{\text{H}_2, \text{pd}}$ in Sec. 3.4.1. By using the one-to-one correspondence between $k_{\text{H}^-, \text{pd}}/k_{\text{H}_2, \text{pd}}$ and J^{crit} and the approximate relation between $k_{\text{H}^-, \text{pd}}$ and $J_{2\text{eV}}$, we have proposed a formula given by Eqs. (26), (28) and (31) to estimate J^{crit} . With this formula, J_{crit} is reproduced with at most 30% error from the information of $J_{2\text{eV}}/J_{\text{LW}}$ for the realistic and black-body spectra studied in this paper.

Let us discuss the implication of our results. In the followings, we adopt $J_{\text{LW},21}^{\text{crit}} = 1400$ as the fiducial value, because it is the typical value for young and metal-poor galaxies commonly present in the supposed DCBH formation era at $z \gtrsim 10$. It has been known that the value of J^{crit} is much higher than the averaged cosmic LW background $J_{\text{bg}, \text{LW},21} \lesssim 0.1$ in the whole history of the Universe (see, e.g., O’Shea & Norman (2008); Johnson et al. (2013a)), and thus the clouds need to be irradiated by unusually nearby and/or strong sources to achieve $J_{\text{LW}} > J_{\text{LW},21}^{\text{crit}}$. By performing semi-analytical computations with N-body simulations (A12) and Monte-Carlo simulations (D14), A12 and D14 estimated the DCBH number density n_{DCBH} with assumption that DCBHs are formed in all the atomic-cooling halos with $J_{\text{LW}} > J_{\text{LW},21}^{\text{crit}}$. However, they may have overestimated n_{DCBH} due to the smaller values of J^{crit} used in their estimation ($J_{\text{LW},21}^{\text{crit}} = 30$ and 300 are used in A12 and D14, respectively).

We re-estimate n_{DCBH} with our $J_{\text{LW},21}^{\text{crit}} = 1400$ by extrapolating the results of A12 and D14. The estimate of n_{DCBH} changes from $n_{\text{DCBH}} \sim 10^{-7} \text{ cMpc}^{-3}$ to $n_{\text{DCBH}} \sim 10^{-10} \text{ cMpc}^{-3}$ at $z = 10$ according to Fig. C1 of D14, and from $n_{\text{DCBH}} \sim 10^{-4} \text{ cMpc}^{-3}$ to $n_{\text{DCBH}} \sim 10^{-6} \text{ cMpc}^{-3}$ at $z = 12$ according to Fig. 7 of A12. Although the values of n_{DCBH} estimated according to D14 and A12 do not match each other, both decrease by two or three orders of magnitude. The observed high-redshift SMBH number density is $n_{\text{SMBH}} \sim 10^{-9} \text{ cMpc}^{-3}$ at $z \sim 6$ (Fan et al. (2001); Vene-

mans et al. (2013)), which is in the same order as n_{DCBH} estimated according to D14. In order to test the scenario of SMBH formation via DCBH by comparing predicted n_{DCBH} and observed n_{SMBH} , it is crucial to more precisely estimate n_{DCBH} in the light of our $J_{\text{LW},21}^{\text{crit}} = 1400$. We would like to note that the present-day SMBH number density inferred from observed luminosity function of active galactic nuclei is $n_{\text{SMBH}} \sim 10^{-4} \text{ cMpc}^{-3}$ (Shankar et al. (2009); Johnson et al. (2013b)), which is several orders of magnitude higher than our estimate of n_{DCBH} , and it is thus unlikely that all of the SMBHs are originated from DCBHs.

In order to achieve such strong external radiation as $J_{\text{LW},21} \gtrsim 1400$, source galaxies need to be very close to the DCBH-forming halos. In such cases, we expect that dynamical interactions between the sources and clouds cannot be overlooked, and thus the above extrapolation of the results of A12 and D14 may be no longer correct. One possibility is large fraction of the pairs merge to single larger halos due to the gravitational interactions before forming DCBHs, as suggested by cosmological simulations (Chon et al. in prep.). Another is that radiation from one of pairs of halos to another realizes $J_{\text{LW},21} > 1000$ during the synchronized evolution of the pairs (Visbal et al. (2014b)). In any case, it is necessary to understand how strong external radiation $J_{\text{LW},21} \gtrsim 1400$ is realized, by studying further about the effects of interactions between primordial-gas clouds and radiation sources.

In this paper, we have studied the dependence of J^{crit} on spectra of external radiation. However, J^{crit} also depends on other physical conditions of the clouds and their environment. Inayoshi & Omukai (2011) found that J^{crit} increases in the presence of cosmic-ray and/or X-ray, although it is not clear yet how much cosmic-ray and/or X-ray are emitted from the same galaxy as the source of radiation. Omukai et al. (2008) found the conditions on metallicity allowed to form DCBHs, although it is not yet clear how J^{crit} changes in the case that the metallicity is very small but not exactly zero. D14 and Agarwal et al. (2014) phenomenologically took into account the effect of metal-enrichment from the same galaxy as the source of radiation in their simulations. S10 and Latif et al. (2014) found that J^{crit} has an order-of-magnitude scatter due to three-dimensional structures of the clouds, such as shocks and turbulence. R14 argued that self-shielding of the LW photons is suppressed by the turbulence in the clouds due to the Doppler broadening of lines. On the other hand, the LW photons irradiated on the clouds may be reduced by the Lyman series absorption of neutral hydrogen in the IGM.

In future studies, it is important to determine the probability distribution of J^{crit} , considering various physical conditions of clouds and their environment. By comparing n_{DCBH} predicted with such probability distribution and observed n_{SMBH} , high-precision test of the SMBH formation scenario via DCBH becomes possible.

ACKNOWLEDGMENTS

The authors would like to thank K. Toma for fruitful discussions and valuable comments. This work is supported in part by the Grant-in-Aid from the Ministry of Education,

Culture, Sports, Science and Technology (MEXT) of Japan (25287040 KO; 26287034 AKI).

REFERENCES

- Agarwal, B., Dalla Vecchia, C., Johnson, J. L., Khochfar, S., & Paardekooper, J.-P. 2014, ArXiv e-prints, arXiv:1403.5267
- Agarwal, B., Khochfar, S., Johnson, J. L., et al. 2012, MNRAS, 425, 2854 (A12)
- Alvarez, M. A., Wise, J. H., & Abel, T. 2009, ApJ, 701, L133
- Anninos, P., Zhang, Y., Abel, T., & Norman, M. L. 1997, New Astron., 2, 209
- Bromm, V., & Loeb, A. 2003, ApJ, 596, 34
- Dijkstra, M., Ferrara, A., & Mesinger, A. 2014, ArXiv e-prints, arXiv:1405.6743 (D14)
- Dijkstra, M., Haiman, Z., Mesinger, A., & Wyithe, J. S. B. 2008, MNRAS, 391, 1961
- Draine, B. T., & Bertoldi, F. 1996, ApJ, 468, 269
- Fan, X., Narayanan, V. K., Lupton, R. H., et al. 2001, AJ, 122, 2833
- Ferland, G. J., Korista, K. T., Verner, D. A., et al. 1998, PASP, 110, 761
- Ferrarese, L., & Merritt, D. 2000, ApJ, 539, L9
- Galli, D., & Palla, F. 1998, A&A, 335, 403
- Gebhardt, K., Bender, R., Bower, G., et al. 2000, ApJ, 539, L13
- Glover, S. C. O., & Abel, T. 2008, MNRAS, 388, 1627
- Gültekin, K., Richstone, D. O., Gebhardt, K., et al. 2009, ApJ, 695, 1577
- Hollenbach, D., & McKee, C. F. 1979, ApJS, 41, 555
- Hosokawa, T., Omukai, K., & Yorke, H. W. 2012, ApJ, 756, 93
- Hosokawa, T., Yorke, H. W., Inayoshi, K., Omukai, K., & Yoshida, N. 2013, ApJ, 778, 178
- Inayoshi, K., & Omukai, K. 2011, MNRAS, 416, 2748
- . 2012, MNRAS, 422, 2539
- Inayoshi, K., Omukai, K., & Tasker, E. J. 2014, ArXiv e-prints, arXiv:1404.4630
- Inoue, A. K. 2011, MNRAS, 415, 2920
- John, T. L. 1988, A&A, 193, 189
- Johnson, J. L., & Bromm, V. 2007, MNRAS, 374, 1557
- Johnson, J. L., Dalla Vecchia, C., & Khochfar, S. 2013a, MNRAS, 428, 1857
- Johnson, J. L., Whalen, D. J., Li, H., & Holz, D. E. 2013b, ApJ, 771, 116
- Larson, R. B. 1969, MNRAS, 145, 271
- Latif, M. A., Bovino, S., Van Borm, C., et al. 2014, ArXiv e-prints, arXiv:1404.5773
- Leitherer, C., Schaerer, D., Goldader, J. D., et al. 1999, ApJS, 123, 3
- McGreer, I. D., & Bryan, G. L. 2008, ApJ, 685, 8
- Mihajlov, A. A., Ignjatović, L. M., Sakan, N. M., & Dimitrijević, M. S. 2007, A&A, 469, 749
- Milosavljević, M., Bromm, V., Couch, S. M., & Oh, S. P. 2009, ApJ, 698, 766
- Mortlock, D. 2012, Nature, 489, 42
- Nagakura, T., & Omukai, K. 2005, MNRAS, 364, 1378
- Nakauchi, D., Inayoshi, K., & Omukai, K. 2014, ArXiv e-prints, arXiv:1405.6901
- Omukai, K. 2001, ApJ, 546, 635 (O01)
- Omukai, K., Schneider, R., & Haiman, Z. 2008, ApJ, 686, 801
- O’Shea, B. W., & Norman, M. L. 2008, ApJ, 673, 14
- Penston, M. V. 1969, MNRAS, 144, 425
- Regan, J. A., & Haehnelt, M. G. 2009, MNRAS, 396, 343
- Regan, J. A., Haehnelt, M. G., & Viel, M. 2007, MNRAS, 374, 196
- Richings, A. J., Schaye, J., & Oppenheimer, B. D. 2014, ArXiv e-prints, arXiv:1403.6155 (R14)
- Schaerer, D. 2003, A&A, 397, 527
- Shang, C., Bryan, G. L., & Haiman, Z. 2010, MNRAS, 402, 1249 (S10)
- Shankar, F., Weinberg, D. H., & Miralda-Escudé, J. 2009, ApJ, 690, 20
- Shapiro, P. R., & Kang, H. 1987, ApJ, 318, 32
- Stancil, P. C. 1994, ApJ, 430, 360
- Venemans, B. P., Findlay, J. R., Sutherland, W. J., et al. 2013, ApJ, 779, 24
- Visbal, E., Haiman, Z., & Bryan, G. L. 2014a, MNRAS, 442, L100
- . 2014b, ArXiv e-prints, arXiv:1406.7020
- Wolcott-Green, J., & Haiman, Z. 2011, MNRAS, 412, 2603 (WG11)
- Wolcott-Green, J., Haiman, Z., & Bryan, G. L. 2011, MNRAS, 418, 838
- Yahil, A. 1983, ApJ, 265, 1047
- Yue, B., Ferrara, A., Salvaterra, R., Xu, Y., & Chen, X. 2014, MNRAS, 440, 1263